**Science and Technology Indonesia**
*e*-ISSN:2580-4391 *p*-ISSN:2580-4405
Vol. 11, No. 1, January 2026

Research Paper

# Anti-Photoaging Effects of Moisturizer and Serum Containing *Andrographis paniculata*, *Syzygium aromaticum*, and *Pogostemon cablin*: A Network Pharmacology, Molecular Docking, and *in vivo* Study

Oktavia Rahayu Adianingsih[1*], Christopher Kuncoro Johan[1], Widarson[1], Eurica Andriani Najwa Ravsanjani[1], Bershiella Amandari Sutiyono[1], Iffah Qurrotuain[1], Valentina Yurina[1], Oktavia Eka Puspita[1], Dhelya Widasmara[2], Akbar Saitama[3], Didik Hariyono[3]

[1]*Department of Pharmacy, Faculty of Medicine, Universitas Brawijaya, Malang, 65145, Indonesia*
[2]*Department of Dermatology and Venereology, Faculty of Medicine, Universitas Brawijaya, Malang, 65145, Indonesia*
[3]*Department of Agronomy, Faculty of Agriculture, Universitas Brawijaya, Malang, 65145, Indonesia*
***Corresponding author**: oktavia.rahayu@ub.ac.id

**Abstract**
Ultraviolet-B (UVB)-induced photoaging accelerates collagen degradation, disrupts dermal structure, and compromises epidermal integrity. Natural extracts, such as *Andrographis paniculata, Syzygium aromaticum*, and *Pogostemon cablin* demonstrated antioxidant and anti-aging properties to mitigate these damages. This study investigated the protective effects of serum and moisturizer containing *A. paniculata* extract, *S. aromaticum* oil, and *P. cablin* oil on UVB-induced photoaging rats, by integrating network pharmacology and *in vivo* experiment. Compounds and photoaging-associated targets were retrieved through online databases. Enrichment analyses were performed using Metascape. Protein-protein interaction (PPI) construction and herbs-compounds-targets-pathways-disease network were performed using STRING and Cytoscape 3.10.0, respectively, followed by molecular docking. An *in vivo* study was conducted to evaluate epidermal thickness, collagen density, and dermo-epidermal junction (DEJ) structure. Eleven key phytoconstituents and twelve core targets were identified in anti-photoaging molecular mechanisms using network pharmacology. Molecular docking analysis revealed that 7-O-methylwogonin demonstrated favorable binding against ten photoaging-associated targets. KEGG enrichment analysis showed potential inflammation processes inhibition, including photocarcinogenesis, AGE-RAGE signaling pathway, and TNF-$\alpha$ expression. Furthermore, treatment with serum, moisturizer, or combination of both significantly reduced epidermal thickening and enhanced collagen density compared to the UVB-exposed only group. Although no significant difference was observed in DEJ interdigitation index across groups, treated groups exhibited a trend towards better preservation of DEJ structure relative to the UVB group. In summary, serum and moisturizer containing *A. paniculata, S. aromaticum*, and *P. cablin* extracts demonstrated potential anti-photoaging effects by reducing epidermal thickness and preserving collagen density in UVB-exposed rats. These findings support these botanical-based formulations potential as effective anti-aging skincare.

**Keywords**
Andrographis Extract, Clove Oil, Network Pharmacology, Patchouli Oil, Photoaging

Received: 20 July 2025, Accepted: 6 October 2025
https://doi.org/10.26554/sti.2026.11.1.19-35

## 1. INTRODUCTION

Skin aging is a complex biological process that involves a gradual deterioration of structural and functional integrity, driven by a combination of intrinsic and extrinsic factors (Charles-De-Sá et al., 2020; Mohiuddin, 2019). Intrinsic aging, governed by genetic, hormonal, and metabolic mechanisms, is an inevitable process associated with chronological age. On the other hand, extrinsic aging, or photoaging, results predominantly from environmental exposures, particularly ultraviolet (UV) radiation with a growing concern of UV index rise over the past 15 years due to various environmental factors (Addas et al., 2021). Among the various wavelengths, ultraviolet-B (UVB) radiation, spanning 290-320 nm, exhibits the highest bioactivity, penetrating the epidermis and initiating a cascade of deleterious molecular events (Cavinato et al., 2017; Damayanti et al., 2023).

Chronic UVB exposure disrupts skin microenvironment homeostasis by stimulating reactive oxygen species (ROS) overproduction, upregulating mitogen-activated protein kinase (MAPK) activity, and triggering apoptosis, which in turn activate critical transcriptional regulators such as nuclear factor-

kappa B (NF-$\kappa$B) and activator protein-1 (AP-1) (Hani et al., 2023). The activation of these pathways culminates in matrix metalloproteinases (MMPs) upregulation, particularly MMP-1, MMP-3, and MMP-9, enzymes responsible for collagen and elastin degradation within the extracellular matrix (ECM) (Feng et al., 2024; Freitas-Rodríguez et al., 2017). Collagen, a principal component of dermal ECM, predominantly composed of types I (80-90%) and III (8-12%), imparts tensile strength and structural support to the skin. Its fragmentation and degradation triggered by UV irradiation results in visible clinical manifestations such as wrinkles, impaired skin elasticity, and compromised skin barrier, hallmarks of photoaged skin (Liu et al., 2024).

Efforts to ameliorate UVB-induced photodamage have historically included invasive interventions such as hyaluronic acid, laser therapy, and dermal fillers (Urdiales-Gálvez et al., 2019). Nevertheless, there is an increasing consumer preference towards non-invasive, safer, and more sustainable alternatives. In this context, the application of topical formulations containing natural bioactive compounds has received growing scientific interest (Ferreira et al., 2021; Sharma et al., 2022). Botanical extracts are recognized for their multiple pharmacological activities, including antioxidant, anti-inflammatory, and photoprotective properties, offering a promising adjunctive strategy for skin anti-aging interventions (Pangestuti et al., 2021).

Among the botanical agents that have been studied for their dermocosmetic potential are *Andrographis paniculata, Syzygium aromaticum* (clove), and *Pogostemon cablin* (patchouli). *Andrographis paniculata* is particularly valued for its major phytoconstituent andrographolide, which exhibits inhibitory effects on UVB-induced MMP expression, supports ECM preservation, and inhibits ROS-mediated signaling pathways, namely ERK and p38 (Manosalva et al., 2025; Zhan et al., 2016). *Syzygium aromaticum* contains eugenol, a potent free radical scavenger, which mitigates oxidative stress, downregulate MMP expression, reinforces skin barrier integrity, and enhances collagen synthesis pathways via transforming growth factor-beta (TGF-$\beta$)/Smad signaling modulation (Hwang et al., 2018; Kim et al., 2019). Furthermore, *Pogostemon cablin* provides patchouli alcohol, an active metabolite shown to attenuate ROS-mediated dermal degradation, improve dermal fibroblast viability, and downregulating MMPs, particularly MMP-1 and MMP-3 (Feng et al., 2014; Harnelly et al., 2025).

Despite the documented individual benefits of these phytochemicals, combined synergistic effects within topical formulations remains limited and primarily relied on *in vitro* models without *in vivo* histological assessments (Gao et al., 2021; Wang et al., 2020, 2016). In addition, the comparative performance between serum, moisturizer, and their combination products incorporating these extracts remains insufficiently addressed, leaving a significant knowledge gap in the field. Given this context, there is a growing interest in investigating whether topical formulations containing *Andrographis paniculata* extracts, clove oil, and patchouli oil confer protective effects against UVB-induced skin damage. Such an evaluation should encompass objective histological parameters, particularly collagen density, epidermal thickness, and DEJ interdigitation index, within an *in vivo* model of photoaging.

Accordingly, this study aims to assess the anti-photoaging efficacy of serum and moisturizer products, either applied as a single treatment or in combination, formulated with these three botanical extracts. By addressing the gap in current literature through *in vivo* evaluation and by leveraging histological endpoints, this study intends to substantiate the scientific rationale for integrating these natural bioactives into next-generation anti-aging skincare products. In this study, we also explore the synergistic mechanism of these herbs against skin photoaging using network pharmacology. The findings are anticipated to provide critical insights into the synergistic interactions among phytochemicals, thereby contributing to the advancement of dermocosmetic innovations grounded in natural product research.

## 2. EXPERIMENTAL SECTION

### 2.1 Materials and Instrumentation

Materials used for *in silico* study included computer tools with 8th generation Intel Core i5 and Windows 10 Professional 64-bit operational system. Compound retrieval was conducted using PubChem (https://pubchem.ncbi.nlm.nih.gov/). Pharmacokinetic screening of the phytoconstituents was performed using SwissADME (http://www.swissadme.ch/). SwissTargetPrediction (STP, http://www.swisstargetprediction.ch/) and Similarity Ensemble Approach (SEA) search server (https://sea.bkslab.org/) were utilized to predict targets related to the phytoconstituents, while identification of photoaging-related targets was performed using GeneCards (https://www.genecards.org/) and Online Mendelian Inheritance in Man (OMIM, https://www.omim.org/).

Subsequently, protein-protein interaction (PPI) network was constructed using Search Tool for the Retrieval of Interacting Genes/Proteins (STRING, https://string-db.org/). Gene Ontology (GO) and Kyoto Encyclopedia of Genes and Genomes (KEGG) enrichment analyses were performed utilizing Metascape (https://metascape.org). Enrichment results were visualized using SRplot (https://www.bioinformatics.com.cn/srplot). Simultaneously, network connecting the herb s, phytoconstituents, pathways, targets, and disease, was constructed using Cytoscape 3.10.0 software.

An *in silico* molecular docking simulation was carried out using PyRx software version 0.8. Proteins collected from RCSB Protein Data Bank (https://www.rcsb.org/). Geometric validation through Ramachandran favored values was performed using MolProbity (https://molprobity.biochem.duke.edu/), while the distance between natural and docked position of the native ligands was predicted using Zhang Lab's DockRMSD (https://zhanggroup.org/DockRMSD/). Docking visualization was conducted using BIOVIA Discovery Studio software version v24.1.0.23298. For the *in vivo* study, moisturizer and serum containing *A. paniculata* extracts, clove oil, and patchouli oil were provided by PT Skinpharma Teknolo

gi Indonesia. H&E staining reagents were obtained from Leica Biosystems (Wetzlar, Germany), while Masson's Trichrome staining was performed using the Trichrome Stain Kit (Modified Masson's) from ScyTek Laboratories (Logan, USA). The instruments used in this study were an Expo Terra Reptile UVB100 25-watt lamp (Rolf C. Hagen Inc., CA, USA), Optilab microscope biology trinocular (Miconos, Yogyakarta, Indonesia), and Optilab Advance + digital camera microscope (Miconos, Yogyakarta, Indonesia).

## 2.2 Methods

### 2.2.1 Retrieval of Phytoconstituents and Target Prediction

The design of this study is depicted in Figure 1. A combination of network pharmacology and molecular docking was performed following methodologies described in previous studies (Deng et al., 2024; Mutiah et al., 2024; Xu et al., 2023). Chemical constituents of the *Andrographis paniculata, Pogostemon cablin*, and *Syzygium aromaticum* were sourced from previous studies. Andrographolides from *Andrographis paniculata* were andrograpanin, andrographiside, andrographolide, bis-andrographolide, isoandrographolide, neoandrographolide, 14-deoxy-11-oxoandrographolide, 14- deoxy-11,12- didehydroandrographolide, and 14- deoxyandrographolide (Intharuksa et al., 2022). In addition, flavonoids extracted from Andrographis paniculata were 5,7,2',3'-tetramethoxyflavone, 5- hydroxy- 7,2',3'-trimethoxyflavone, 7-O-methylwogonin, flavone-1,2' methylether, 5-hydroxy -7,8,2',5'- tetramethoxyfla vone, and dihydroskullcapflavone (Chauhan et al., 2019). Meanwhile, compounds derived from *Pogostemon cablin* essential oil included $\alpha$-pinene, $\beta$-pinene, $\alpha$-limonene, $\beta$-patchoulene, $\beta$-elemene, $\beta$-gurjunen, $\beta$-caryophyllene, $\alpha$-guaiene, seychellene, $\alpha$-humulene, $\alpha$-patchoulene, $\beta$-selinene, ledene, $\alpha$-selinene, $\alpha$-bulnesene, caryophyllene oxide, globulol, 5-epi-7-epi-a-eudesmol, and patchouli alcohol (Galovičová et al., 2022). Furthermore, the phytoconstituents of *Syzygium aromaticum* comprised eugenol, $\beta$-caryophyllene, $\alpha$-humulene, eugenol acetate, $\alpha$-copaene, chavicol, methyl salicylate, 4-allylanisole, and benzyl acetate (Pandey et al., 2024).

Compound SMILES were obtained from PubChem. Pharmacokinetic properties and drug-likeness of the compounds were assessed using SwissADME (Daina et al., 2017). Pharmacokinetic parameters, such as molecular weight (MW), hydroge n-bond donor (HBD), hydrogen-bond acceptor (HBA), and consensus log P (clogP) were evaluated in accordance with the Lipinski's Rule of Five. Compounds exhibiting one or less Lipinski's Rule of Five violation, Topological Polar Surface Area (TPSA) below 140 Å, and an oral bioavailability over 10% were selected for further investigation (Benet et al., 2016). Subsequently, target genes of these eligible compounds were predicted using STP and SEA, with the search limited to Homo sapiens. Duplicate targets yielded by both databases were removed. Photoaging-related targets were predicted using GeneCards and OMIM. Duplicated photoaging-related targets were removed. Subsequently, the intersection of compounds- and photoaging-related targets domains were determined using a Venn diagram modelled with the SRplot.

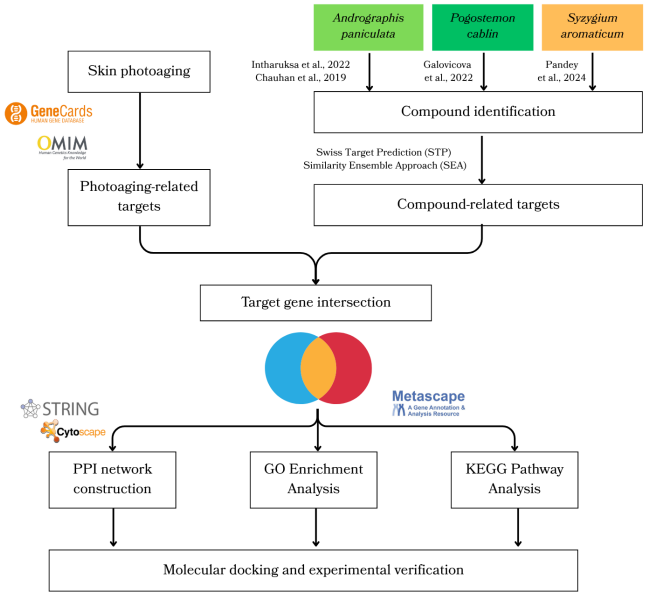


**Figure 1.** Study Flowchart

### 2.2.2 Protein-Protein Interaction (PPI) Network and Enrichment Analysis

The obtained overlapping targets were subsequently analyzed using the STRING, as performed in a previous study (Han et al., 2022a). The PPI network was constructed on medium confidence score (0.400) and FDR stringency (5%). Interactions between core protein targets were visualized using Cytoscape software version 3.10.0. CytoHubba plug-in was utilized to reveal top 20 proteins with the highest degree in the PPI network. GO and KEGG enrichment analysis were conducted using Metascape. Visualization of the top biological processes (BP), cellular components (CC), molecular functions (MF), and KEGG pathways were visualized as bubble plots using SRplot.

### 2.2.3 Herbs-Compound-Target-Pathway-Disease (H-C-T-P-D) Network

The network explaining interactions between herbs, phytoconstituents, overlapping targets, pathways, and skin photoaging was generated using Cytoscape software version 3.10.0 (Adianingsih et al., 2024). The top ten proteins and compounds with the highest degree in the network were selected for subsequent analysis.

### 2.2.4 Molecular Docking Analysis and Visualization

3D structures of the selected phytoconstituents were retrieved from PubChem. OpenBabel 3.0.1 was used for format conversion (SDF to PDB). Crystal structures of the selected target proteins were obtained from the RCSB Protein Data Bank. Each crystal structure was sterilized, and the native ligand was isolated using PyMOL software version 0.8. Sterilized proteins

were geometrically validated using Ramachandran favored values using MolProbity. Proteins with >90% Ramachandran favored score were considered ideal for further analysis (Hema et al., 2021).

The molecular docking simulations were carried out using PyRx software version 0.8. Root mean square deviation (RMSD) value between natural and docked conformations of each native ligand was calculated using Zhang Lab's Dock-RMSD. Calculated results with RMSD values less than 3.0 Åwere considered ideal for further analysis (Jain and Nicholls, 2008). Favorability of the docking results was primarily identified through the binding affinities between the selected phytoconstituents and proteins, where discretions were made into strong predicted binding (≤ -7 kcal/mol), moderate predicted binding (≤ -5 kcal/mol), and no predicted binding (>-5 kcal/-mol) (Wong et al., 2022). Amino acid interactions between phytoconstituents and proteins with high binding affinities were visualized using BIOVIA Discovery Studio v24.1.0.23298.

#### 2.2.5 Animals and UV-B Irradiation

The methodological approach for the *in vivo* study was adapted from a previous study (Anjum et al., 2023). Twenty-five male Wistar rats (6–7 weeks old; 100–150 grams) were maintained under temperature- and light-controlled conditions (25 ± 2 °C, 12-h light/dark cycle) with food and water provided *ad libitum*. Ethical approval was obtained from the Ethics Committee of the Faculty of Medicine, Universitas Brawijaya, Indonesia, with approval number of 271/EC/KEPK/09/2023. The rats were acclimated for seven days before the investigation at the Laboratory of Pharmacology, Faculty of Medicine, Universitas Brawijaya. Subsequently, animals were randomly divided into five groups ($n$ = 5 per group). The dorsal hair of the rats was shaved to a 4 × 5 $cm^2$ area. Irradiation was performed using an Expo Terra Reptile UVB100 25-watt lamp with an emission spectrum between 290-320 nm. Group I served as the normal group and received no UV-B exposure. Group II (positive control) received only UV-B radiation. Groups III, IV, and V were irradiated with UV-B and then topically treated with moisturizer, serum, and a combination of both, respectively. Products were applied topically five minutes before UV-B radiation. UV-B radiation was carried out for three weeks, with exposure on five consecutive days each week. The exposure time was gradually increased. Initially, animals were exposed to UV-B radiation for 10 minutes per day, then the second week for 15 minutes per day, and increased to 20 minutes per day in the third week. At the end of treatments, rats were euthanized by cervical dislocation, and skin specimens were harvested for further histological analysis.

#### 2.2.6 Histopathological Analysis

Hematoxylin-eosin (H&E) and Masson's Trichrome staining were carried out in the Laboratory of Pathology Anatomy, Faculty of Medicine, Universitas Brawijaya. In brief, the skin was fixed in 10% neutral-buffered formalin, embedded in paraffin, and sectioned at a thickness of 4 $\mu$m. The samples were then deparaffinized, rehydrated, and stained with H&E or Masson's trichrome. H&E staining was utilized to observe the skin structure and epidermal thickness, while Masson's trichrome staining was employed to evaluate the density of collagen fibers in the dermis (Dibal et al., 2022; Xu and Zhao, 2022). Variables were analyzed at five random locations per slide using an Optilab trinocular biology microscope. Histology analysis in H&E staining uses 400× magnification, while histology analysis in Masson's trichrome staining uses 100× magnification. Each specimen was photographed under the Optilab Advance+ digital camera microscope with Optilab Viewer software. Epidermal thickness was measured using Optilab Viewer software, which had already been calibrated. Collagen density was evaluated using the ImageJ software version 1.53e (National Institutes of Health, Maryland, USA).

#### 2.2.7 Statistical Analysis

All data were presented as the mean ± standard deviation (SD). Statistical analysis was performed using one-way analysis of variance (ANOVA) followed by Tukey's HSD test. A p-value less than 0.05 was considered statistically significant. Analyses were conducteda using the SPSS software (version 25.0, SPSS Inc., Chicago, IL, USA).

## 3. RESULTS AND DISCUSSION

### 3.1 Predicted Compound-and Photoaging-Related Targets

A total of 43 compounds were identified from previous literatures. Notably, two identical compounds; $\alpha$-humulene and $\beta$-caryophyllene were found in both *Pogostemon cablin* and *Syzygium aromaticum*. Pharmacokinetic properties of the 41 unique compounds were detailed in Table 1. Principally, Lipinski's rule of five is widely utilized to predict the pharmacokinetic profiles of a compound through several criteria. Compounds with <500 Da molecular weight, <5 hydrogen bond donors, <10 hydrogen bond acceptors, and <5 calculated log P value with no more than one violation of the criteria are predicted to possess favorable absorption and permeability profiles (Benet et al., 2016). Simultaneously, topological polar surface area (TPSA), a renowned parameter to predict intestinal and blood-brain barrier permeability of a compound, is also incorporated in this study, where the preferred TPSA value should fall below the cutoff (140 Å) (Whitty et al., 2016). Furthermore, prediction of bioavailability scores was performed through SwissADME, where compounds with >10% bioavailability score are considered as ideal drug candidates (Daina et al., 2017). Subsequently, two andrographolides of *Andrographis paniculata* were excluded for exceeding one violation of the Lipinski's Rule of Five, while two additional flavonoids of *Andrographis paniculata* were removed from analysis due to unavailable SMILES. Ultimately, 37 phytoconstituents of the three herbals were highlighted for further assessment.

Prediction of compound-related target proteins using STP and SEA databases identified 679 and 504 unique proteins, respectively. Following the removal of the duplicates, 1,096 compound-related targets were obtained. In parallel, GeneCard

**Table 1.** Drug-Likeness Analysis of the 37 Unique Compounds

| Compounds | PubChem CID | SMILES | Lipinski's Rule of Five Criteria | | | | | TPSA | Bioavailability | Yes/ No |
|---|---|---|---|---|---|---|---|---|---|---|
| | | | MW | HBA | HBD | clogP | Violation | | | |
| Andrographanin | 11666871 | P | 318.45 | 3 | 1 | 3.95 | 0 | 46.53 | 0.55 | Yes |
| Andrographiside | 44595338 | P | 512.59 | 10 | 6 | 0.31 | 1 | 166.14 | 0.17 | No |
| Andrographolide | 5318517 | P | 350.45 | 5 | 3 | 2.33 | 0 | 86.99 | 0.55 | Yes |
| bis-Andrographolide | 12000602 | P | 684.57 | 8 | 4 | 2.42 | 1 | 133.52 | 0.55 | No |
| Isoandrographolide | 101243415 | P | 350.45 | 5 | 2 | 2.42 | 0 | 75.99 | 0.55 | Yes |
| Neoandrographolide | 9848042 | P | 480.59 | 8 | 4 | 2.33 | 0 | 125.68 | 0.55 | Yes |
| 14-deoxy-11-oxoandrographolide | 9958003 | P | 348.43 | 5 | 3 | 2.07 | 0 | 83.83 | 0.55 | Yes |
| 14-deoxy-11,12-didehydroandrographolide | 5708351 | P | 332.43 | 4 | 2 | 3.07 | 0 | 66.76 | 0.55 | Yes |
| 14-deoxyandrographolide | 11624161 | P | 334.45 | 4 | 2 | 3.15 | 0 | 66.76 | 0.55 | Yes |
| 5,7,2',3'-tetramethoxyflavone | – | P | 344.34 | 6 | 0 | 3.55 | 0 | 67.13 | 0.55 | Yes |
| 5-hydroxy-7,2',3'-trimethoxyflavone | 12315219 | P | 328.33 | 7 | 1 | 2.91 | 0 | 78.13 | 0.55 | Yes |
| 7-O-methylwogonin | 188136 | P | 298.29 | 5 | 1 | 2.81 | 0 | 68.9 | 0.55 | Yes |
| Flavone-1,2'-methyl ether | – | – | – | – | – | – | – | – | – | No |
| 5-hydroxy-7,8,2',5'-tetramethoxyflavone | 10948318 | P | 358.34 | 7 | 1 | 2.83 | 0 | 87.36 | 0.55 | Yes |
| Dihydroxycalcapliflavone | – | – | – | – | – | – | – | – | – | No |
| $\alpha$-Pinene | 11240513 | P | 136.23 | 0 | 0 | 3.42 | 0 | 0.00 | 0.55 | Yes |
| $\beta$-Pinene | 440967 | P | 136.23 | 0 | 0 | 3.42 | 0 | 0.00 | 0.55 | Yes |
| $\alpha$-Limonene | 91496 | P | 152.23 | 1 | 0 | 2.71 | 0 | 12.53 | 0.55 | Yes |
| $\beta$-Patchoulene | 1017531 | P | 204.35 | 0 | 0 | 4.4 | 1 | 0 | 0.55 | Yes |
| $\beta$-Elemene | 6918391 | P | 204.35 | 0 | 0 | 4.65 | 1 | 0 | 0.55 | Yes |
| $\alpha$-Gurjunene | 521243 | P | 204.35 | 0 | 0 | 4.27 | 1 | 0 | 0.55 | Yes |
| $\beta$-Caryophyllene | 5281515 | P | 204.35 | 0 | 0 | 4.35 | 1 | 0 | 0.55 | Yes |
| $\alpha$-Guaiene | 107512 | P | 204.35 | 0 | 0 | 4.29 | 1 | 0 | 0.55 | Yes |
| Seychellene | 519743 | P | 204.35 | 0 | 0 | 4.49 | 1 | 0 | 0.55 | Yes |
| $\alpha$-Humulene | 528150 | P | 204.35 | 0 | 0 | 4.51 | 1 | 0 | 0.55 | Yes |
| $\alpha$-Patchoulene | 521710 | P | 204.35 | 0 | 0 | 4.39 | 1 | 0 | 0.55 | Yes |
| $\beta$-Selinene | 519361 | P | 204.35 | 0 | 0 | 4.5 | 1 | 0 | 0.55 | Yes |
| Ledene | 10910653 | P | 204.35 | 0 | 0 | 4.26 | 1 | 0 | 0.55 | Yes |
| $\alpha$-Selinene | 10123 | P | 204.35 | 0 | 0 | 4.4 | 1 | 0 | 0.55 | Yes |
| $\alpha$-Bulnesene | 9427 | P | 204.35 | 0 | 0 | 4.31 | 1 | 0 | 0.55 | Yes |
| Caryophyllene oxide | 17422010 | P | 220.35 | 1 | 1 | 3.68 | 0 | 12.53 | 0.55 | Yes |
| Globulol | 12304985 | P | 222.37 | 1 | 1 | 3.41 | 0 | 20.23 | 0.55 | Yes |
| 5-epi-7-epi-$\alpha$-eudesmol | 6428428 | P | 222.37 | 1 | 1 | 3.41 | 0 | 20.23 | 0.55 | Yes |
| Patchouli alcohol | 10955174 | P | 222.37 | 1 | 1 | 3.56 | 0 | 20.23 | 0.55 | Yes |
| Eugenol | 3314 | P | 164.2 | 2 | 1 | 2.25 | 0 | 29.46 | 0.55 | Yes |
| Eugenol acetate | 7136 | P | 206.24 | 3 | 0 | 3.4 | 0 | 35.53 | 0.55 | Yes |

| | | | | | | | | | | |
|---|---|---|---|---|---|---|---|---|---|---|
| $\alpha$-Copaene | 19725 | P | 204.35 | 0 | 0 | 4.3 | 1 | 0 | 0.55 | Yes |
| Chavicol | 68148 | P | 134.18 | 1 | 1 | 2.33 | 0 | 20.23 | 0.55 | Yes |
| Methyl salicylate | 4133 | P | 152.15 | 3 | 1 | 1.66 | 0 | 46.53 | 0.55 | Yes |
| 4-Allylanisole | 8815 | P | 148.2 | 1 | 0 | 2.78 | 0 | 9.23 | 0.55 | Yes |
| Benzyl acetate | 8785 | P | 150.17 | 2 | 0 | 1.94 | 0 | 26.3 | 0.55 | Yes |

s and OMIM databases yielded 292 and 171 photoaging-related targets, respectively. Elimination of the duplicates revealed 463 unique photoaging-related target proteins. Consequently, Venn diagram analysis (Figure 2) revealed 82 shared targets common to the two domains.

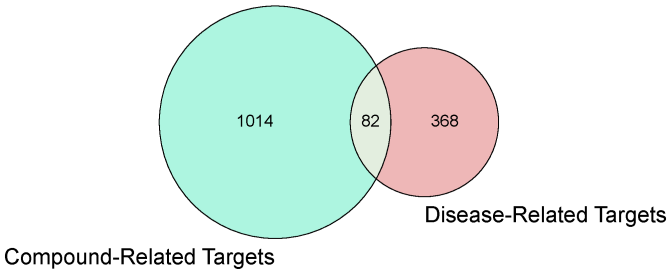


**Figure 2.** Intersection Between Compounds and Photoaging -Related Targets

### 3.2 PPI Network and Enrichment Analysis

PPI network revealed a total of 1,008 edges and 80 nodes (Figure 3A). Two proteins, CHRNA7 and TGM1, showed no interactions with the other proteins. Subsequently, 20 top proteins, ranked by edge count, were identified (Figure 3B). These proteins are CASP3, MAPK8, JUN, MMP9, HIF1A, MAPK1, MTOR, CASP8, PPARG, BCL2L1, TNF, NFKB1, AKT1, ESR1, FOS, IL6, CREB1, CASP9, MAPK3, and EGFR. Darker nodes represent a higher number of degrees in the network.

GO enrichment analysis identified 1,210 BP, 51 CC, and 117 MF associated to the 82 overlapping proteins. The top 10 terms with the lowest logP value are presented in Figure 4, while the top 20 GO terms are visualized as a bubble plot in Figure 5A. In addition, KEGG enrichment analysis yielded 170 pathways linked to the 82 overlapping proteins. The 20 most enriched pathways, ranked by lowest logP value, are illustrated in a bubble diagram (Figure 5B).

The top 20 GO enrichment terms comprised 18 BPs and 2 MFs with the lowest logP value, indicating higher significance of the term within the network (Li et al., 2021). The identified BPs included cellular response to lipid, response to lipopolysaccharide, and cellular response to environmental stimulus, while the MFs encompassed nuclear receptor activity and ligand-activated transcription factor activity. Lipopolysaccharide is widely recognized for its role in promoting inflammation, notably by upregulating TNF-$\alpha$ synthesis (Wang et al., 2025). Lipids also play a critical role in skin photoaging modulation, as shown by a notable reduction in free fatty acid and triglyceride levels in UVB-induced photoaged skin (Kim et al., 2020).

Additionally, nuclear receptor and ligand-activated transcription factor activities were reported among the top MF term in a previous assessment of the anti-photoaging potency of asiaticosides, indicating their importance in herbal-based anti-photoaging activities (Huang et al., 2023). Furthermore, KEGG enrichment analyses showed several pathways modulated by the three herbals within the framework of skin photoaging. UVB radiation is well established as a key factor in photocarcinogenesis-related activities, contributing to the progression of skin photoaging into malignant skin cancer. This process might also disrupt normal apoptosis mechanisms (Bosch et al., 2015). UVB-induced skin photoaging is also associated with the elevated expression of pro-inflammatory mediators, including TNF-$\alpha$ and IL-17, which represent therapeutic targets for skin photoaging (Chen et al., 2024). Additionally, AGE-RAGE signaling activity has been implicated in skin photoaging through its role in increasing melanin production, further positioning it as a promising target for therapeutic intervention (Chmielewski and Lesiak, 2024).

### 3.3 H-C-T-P-D Network Analysis

Figure 6 depicts the interactions among the three herbals, 37 phytoconstituents, 82 overlapping target proteins, 20 top KEGG pathways, and skin photoaging. Topological network analysis identified the top 11 compounds, composed of 4 phytoconstituents of *Andrographis paniculata*, 4 phytoconstituents of *Pogostemon cablin*, and 3 phytoconstituents of *Syzygium aromaticum.* These compounds were 5-hydroxy-7,8,2',5' -tetramet hoxyflavone (28), $\alpha$-selinene (25), $\alpha$-pinene (25), 7-O -methyl wogonin (25), 5,7,2',3'-tetramethoxyflavone (23), $\alpha$- patchoulen e (22), 5-hydroxy-7,2',3'-trimethoxyflavone (22), benzyl acetate (21), $\alpha$-copaene (21), eugenol (19), and patchouli alcohol (19). In addition, top 12 target proteins that showed the highest degree within the network were ESR1 (31), AR (30), MAPK14 (29), MAK3 (27), ESR2 (26), MAPK8 (24), MAPK10 (23), MAPK1 (23), NFKB1 (22), AKT1 (21), PIK3R1 (21), and HSD11B1 (21).

Traditionally, specific phytoconstituents such as andrograph olide for *Andrographis paniculata*, pogostone and patchouli alcohol for *Pogostemon cablin*, and eugenol for *Syzygium aromaticum* have been regarded as the marker compounds of the herbals, potentially primarily associated with the pharmacological properties of these herbals. However, molecular docking analysis revealed that these key phytoconstituents did not exhibit favorable interactions with the skin photoaging-related tar-

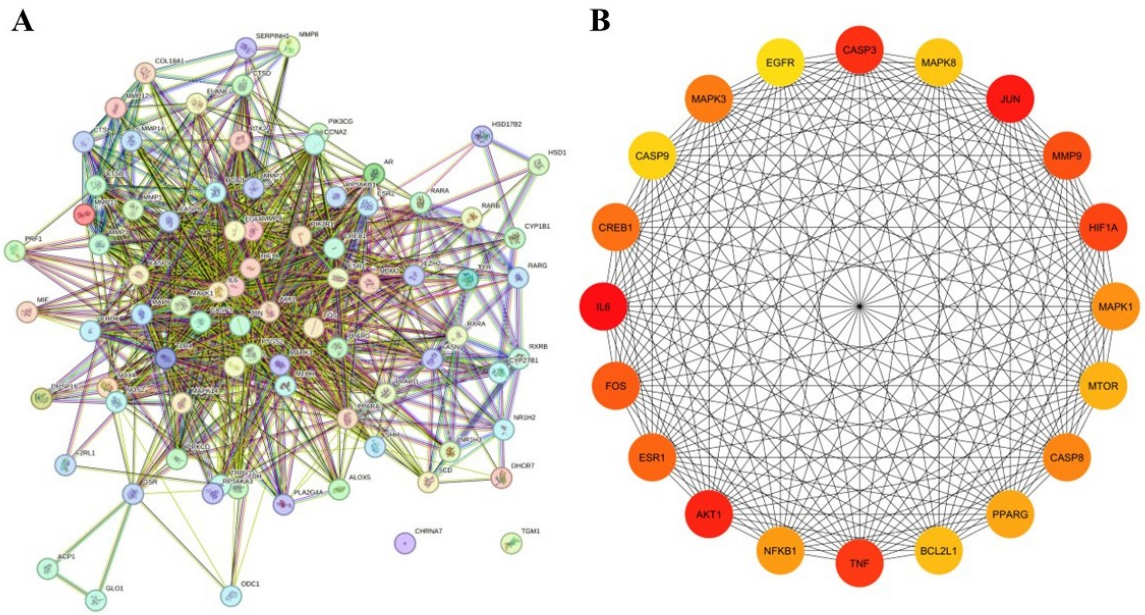


**Figure 3.** PPI Network of the (A) 82 Overlapping Targets and (B) The Top 20 Proteins with the Highest Degree

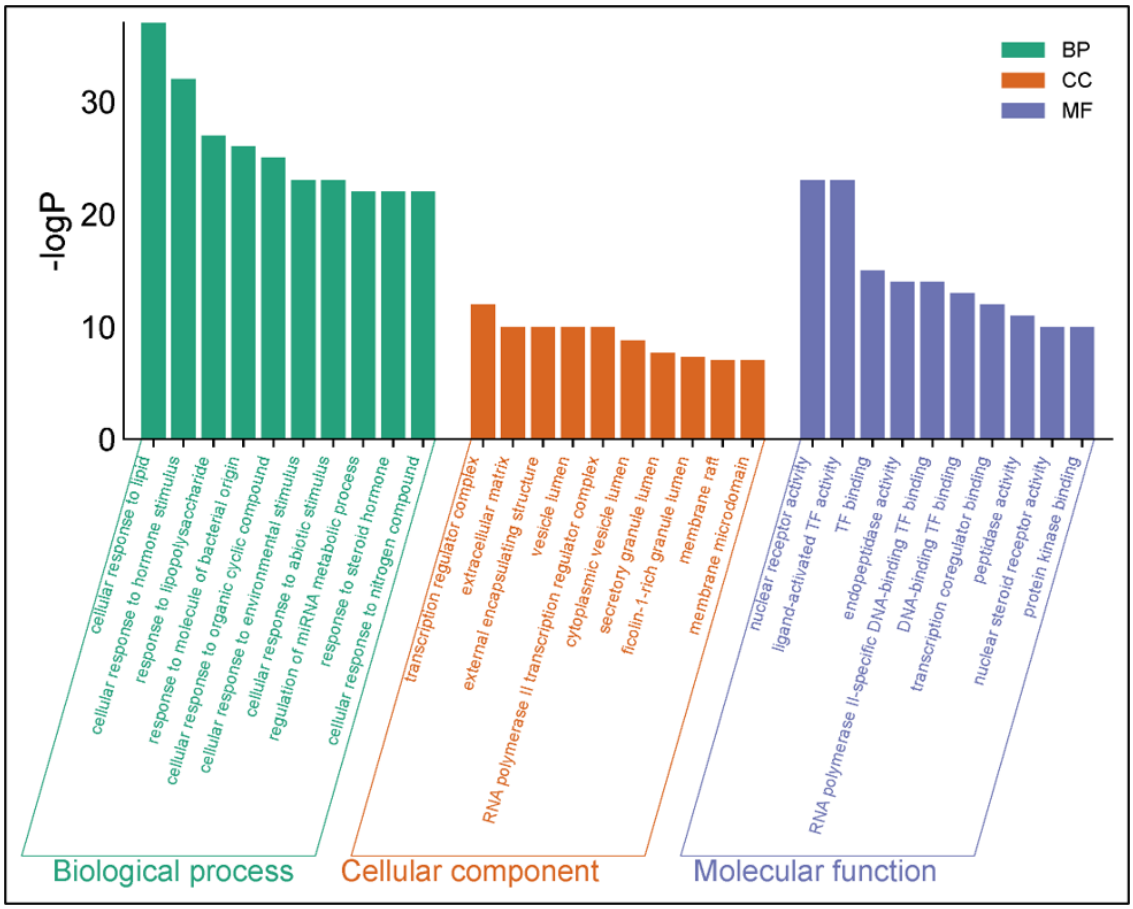


**Figure 4.** The Top 10 Terms of BP, CC, and MF Enrichment Analysis

**Table 2.** Drug-likeness Analysis of the 37 Unique Compounds

| Target Protein Identity | Native Ligand | Ramachandran Favored Value | Center Grid Box | | | Grid Box Size | | |
|---|---|---|---|---|---|---|---|---|
| | | | X | Y | Z | X | Y | Z |
| Estrogen receptor 1 (ESR1) | EST | 92.41% | 106.1636 | 15.0046 | 96.5451 | 5.9402 | 12.6370 | 11.1011 |
| Androgen receptor (AR) | 77U | 96.36% | 26.5120 | 2.3407 | 4.2055 | 9.4990 | 13.2271 | 5.9928 |
| Mitogen-activated protein kinase 14 (MAPK14) | LBE | 96.04% | -0.4217 | 0.3338 | -20.0850 | 14.7933 | 12.0576 | 19.7416 |
| Mitogen-activated protein kinase 3 (MAPK3) | 38Z | 98.28% | 34.7575 | 54.0114 | 51.0380 | 25.0000 | 25.0000 | 25.0000 |
| Estrogen receptor 2 (ESR2) | EST | 98.19% | -26.4867 | 34.9420 | -16.5477 | 6.8936 | 13.3127 | 10.0897 |
| Mitogen-activated protein kinase 8 (MAPK8) | ANP | 98.55% | 11.4868 | 7.5527 | 18.6829 | 10.5860 | 11.0300 | 12.5857 |
| Mitogen-activated protein kinase 10 (MAPK10) | 86C | 92.73% | -4.6496 | 28.6838 | -34.1929 | 18.0263 | 21.9894 | 16.4390 |
| Mitogen-activated protein kinase 1 (MAPK1) | 6H3 | 96.81% | 69.1601 | 14.7068 | 8.9848 | 25.0000 | 25.0000 | 25.0000 |
| Nuclear factor kappa B 1 (NFKB1) | JMR | 97.96% | 8.0207 | -13.7892 | -15.5041 | 25.0000 | 25.0000 | 25.0000 |
| Protein kinase B (AKT1) | G4T | 97.34% | 12.5718 | -15.9876 | -14.9170 | 22.9251 | 16.5522 | 23.1678 |
| Phosphoinositide-3-kinase regulatory subunit 1 (PIK3R1) | 1LT | 97.17% | -1.8596 | -10.0500 | 16.8340 | 17.2878 | 14.3869 | 21.0257 |
| Hydroxysteroid 11-beta dehydrogenase 1 (HSD11B1) | NAP | 95.97% | 56.5763 | 109.5281 | 44.6769 | 12.6251 | 24.2929 | 16.9445 |

gets. Notably, 7-O-methylwogonin and 5-hydroxy-7,2',3'-tetramethoxyflavone, flavonoids extracted from *Andrographis paniculata*, demonstrated the strongest binding affinities across five and four target proteins, respectively. Moreover, 5-hydroxy-7,8,2',5'-tetramethoxyflavone in *Andrographis paniculata* and $\alpha$-copaene in *Syzygium aromaticum* presented favorable binding properties against two target proteins, while 5,7,2',3'- tetramethoxyflavone in *Pogostemon cablin* produced the most stable bond against NFKB1. To date, there is still limited evidence elucidating the role of the other compounds in alleviating skin photoaging, suggesting that phytoconstituents beyond the established marker compounds may contribute significantly to the pharmacological effects of these herbals.

### 3.4 Molecular Docking Simulation

Geometric validation using MolProbity revealed that all proteins exhibit >90% Ramachandran favored value, indicating that the docking model was valid (Table 2). Molecular docking was performed using a specific approach, with the grid box setting adjusted to the native ligand binding site as described in Table 2, while the binding affinities of the docking model are presented in Table 3. Compounds with high binding affinities against its respective protein are written in bold. Among the predicted targets, AKT1 possesses the highest number of high binding affinities against the phytoconstituents (9), while NFKB1 only displayed moderate to low binding affinities. The highest number of high binding affinities are presented by 7-O-methylwogonin (10), while benzyl acetate and eugenol are unable to exert favorable binding affinity values against any predicted targets. Phytoconstituents that produced the most

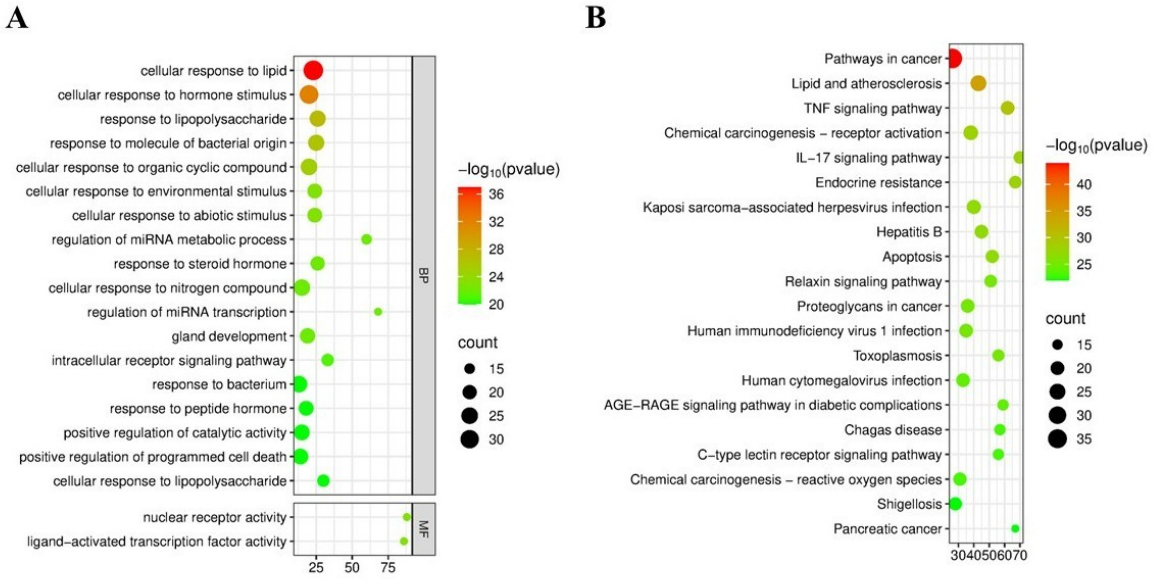


**Figure 5.** Bubble Plots of the Top 20 Terms of (A) GO and (B) KEGG Enrichment Analysis

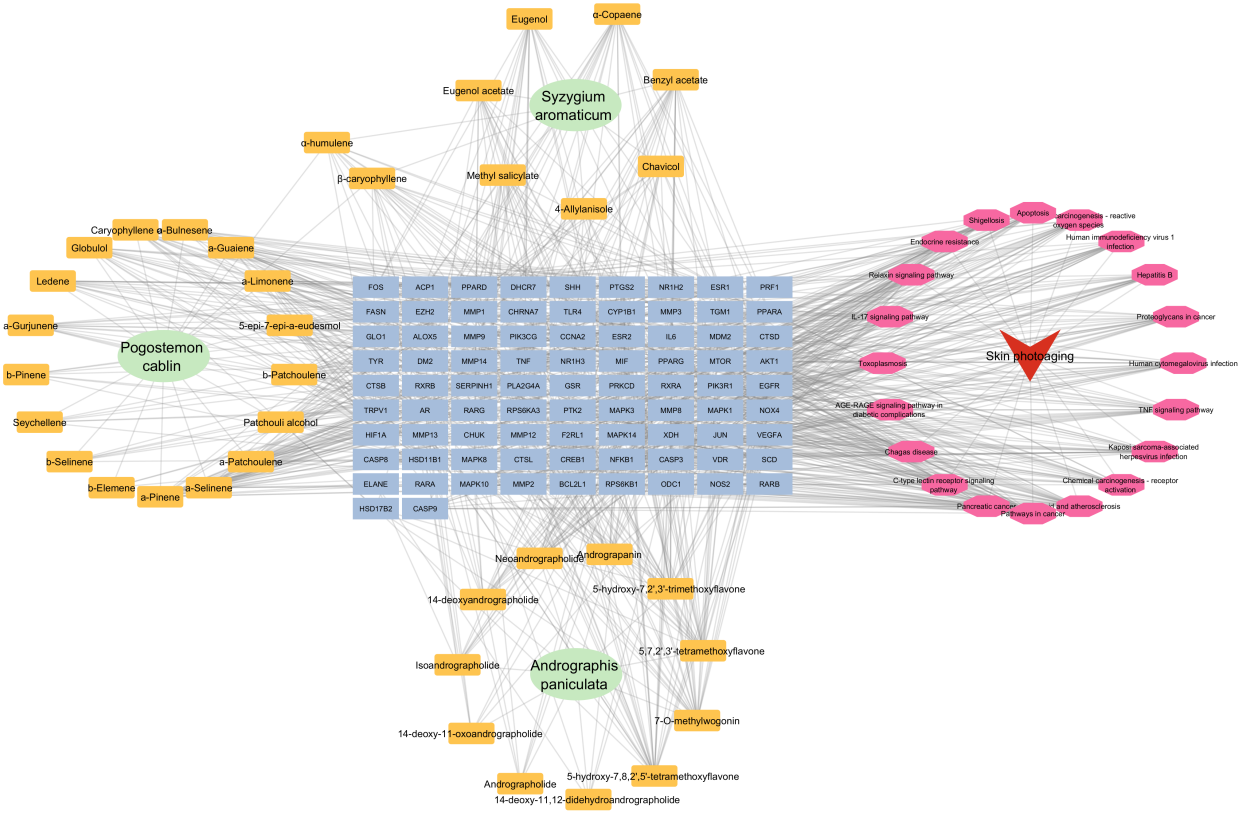


**Figure 6.** H-C-T-P-D Network. Green Ovals Represent the Herbals; Orange Rounded Rectangles Symbolize the Phytoconstituents of the Herbals. Light Blue Rectangles Symbolize the Overlapping Target Proteins. Pink Octagon Shapes Symbolize the Pathways, and the Red V Shape Represent Skin Photoaging

**Table 3.** Binding Affinity and Amino Acid Interactions Over Molecular Docking Simulations

| Compound | Binding Affinity (kcal/mol) | | | | | | | | | | | |
|---|---|---|---|---|---|---|---|---|---|---|---|---|
| | ESR1 | AR | MAPK14 | MAPK3 | ESR2 | MAPK8 | MAPK10 | MAPK1 | NFKB1 | AKT1 | PIK3R1 | HSD11B1 |
| Native | -10.6 | -9.5 | -11.3 | -14.0 | -11.3 | -8.5 | -10.2 | -7.6 | -10.0 | -13.9 | -10.4 | -11.8 |
| 5-hydroxy-7,8,2',5'-tetram-ethoxyflavone | -5.8 | -3.6 | -6.2 | -9.0 | -5.7 | -8.0 | -9.0 | -6.8 | -5.4 | -9.0 | -8.5 | -8.5 |
| $\alpha$-Selinene | -8.3 | -7.1 | -8.2 | -7.8 | -7.9 | -7.1 | -7.3 | -6.2 | -5.2 | -8.2 | -7.5 | -6.8 |
| $\alpha$-Pinene | -5.8 | -5.8 | -6.6 | -8.9 | -6.2 | -5.3 | -9.2 | -6.7 | -5.4 | -9.0 | -8.1 | -7.9 |
| 7-O-methylwogonin | -8.1 | -6.1 | -8.1 | -8.9 | -8.0 | -8.5 | -9.2 | -7.0 | -5.4 | -9.0 | -8.1 | -7.9 |
| 5,7,2',3'-tetram-ethoxyflavone | -3.9 | -3.1 | -7.7 | -9.0 | -3.6 | -8.1 | -8.8 | -6.9 | -5.4 | -8.7 | -7.3 | -7.0 |
| $\alpha$-Patchoulene | -7.7 | -4.7 | -6.0 | -6.0 | -7.9 | -5.0 | -8.9 | -6.3 | -4.9 | -7.3 | -6.2 | -7.0 |
| 5-hydroxy-7,2',3'-trimethoxyflavone | -6.8 | -5.4 | -8.6 | -9.3 | -5.0 | -8.3 | -9.0 | -6.9 | -5.3 | -9.0 | -8.1 | -8.6 |
| Benzyl acetate | -5.8 | -5.9 | -6.3 | -6.6 | -5.9 | -5.9 | -5.8 | -6.1 | -4.5 | -9.0 | -8.1 | -6.5 |
| $\alpha$-Copaene | -8.0 | -7.6 | -6.8 | -7.6 | -8.3 | -8.3 | -9.0 | -6.1 | -4.8 | -8.0 | -7.0 | -6.9 |
| Eugenol | -5.9 | -6.0 | -6.3 | -6.2 | -6.1 | -6.2 | -5.9 | -5.6 | -4.2 | -6.5 | -6.0 | -5.7 |
| Patchouli alcohol | -7.8 | -3.5 | -5.8 | -5.4 | -7.8 | -3.9 | -5.1 | -5.9 | -5.0 | -7.6 | -5.7 | -7.1 |

favorable binding affinities with each protein are visualized in Figure 7.

Estrogen receptors have been extensively studied for their role in skin photoaging. Lephart and Naftolin (2022) reported the essential role of estrogen in preserving skin integrity. In the context of skin photoaging, estrogen exerts antioxidant properties through inhibition of ROS and oxidative stress, stimulates the activity of transforming factor-beta (TGF-$\beta$), and enhances skin hydration. Furthermore, estrogen receptors have been investigated for their role in skin inflammation, where the suppression of estrogen receptor-$\beta$ poses as an anti-photoaging target that modulates the expressions of pro-inflammatory mediators, such as COX-2 and MMPs, in photoaged skin (Chang et al., 2010). Similarly, androgen, which serves as the male counterpart to estrogen in female, possesses pivotal role in skin aging. Aging has been linked to reduced testosterone metabolism and elevated tissue-specific androgen sensitivity (Anawalt and Matsumoto, 2022). Consequently, androgen receptor poses as a potential therapeutic target against skin photoaging.

The role of MAPK and NFKB1 has been reported in previous studies. Theoretically, skin photoaging is modulated through three primary pathways: the MAP kinase, NF-$\kappa$B, and nuclear factor of activated T-cells (NFAT) pathways (Fuller, 2019). However, recent reports indicated that these pathways might not act independently; these pathways overlapped to control inflammation-related genes. Upregulated expression of ROS in UVB-induced skin photoaging triggers several processes, including apoptosis and the activation of MAPK pathway (Hani et al., 2023). Generally, MAPK is composed of extracellular signal-regulated kinase (ERK), c-Jun N-terminal kinase (JNK), and p38. Activation of MAPK leads to the induction of c-Fos and the phosphorylation of c-Jun through JNK and p38. Phosphorylated c-Jun and c-Fos will undergo heterodimerization, forming the AP-1 which is responsible in the collagen degradation (Han et al., 2022b).

In this study, several MAPKs were reported to exert central role in the anti-photoaging activities of the three herbals. Gong et al. (2018) presented MAPK1 role in weakened wound healing ability in UVB-induced skin photoaging. MAPK1 and

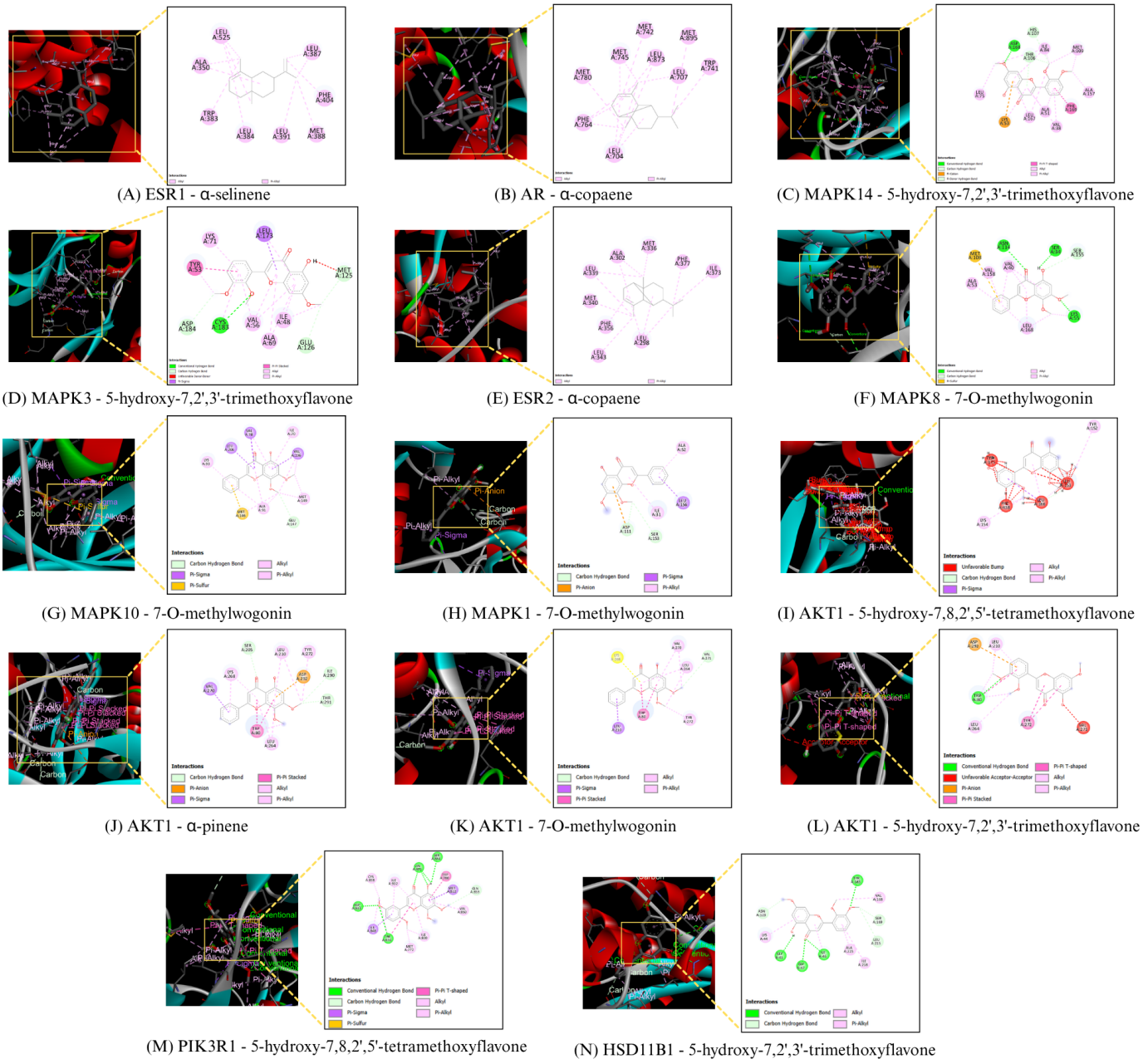


**Figure 7.** Docking Visualization of (A) ESR1 and α-Selinene; (B) AR and α-Copaene; (C) MAPK14 and 5-Hydroxy-7,2',3'-Trimethoxyflavone; (D) MAPK3 and 5-Hydroxy-7,2',3'-Trimethoxyflavone; (E) ESR2 and α-Copaene; (F) MAPK8 and 7-O-Methylwogonin; (G) MAPK10 and 7-O-Methylwogonin; (H) MAPK1 and 7-O-Methylwogonin; (I) AKT1 and 5-Hydroxy-7,8,2',5'-Tetramethoxyflavone; (J) AKT1 and α-Pinene; (K) AKT1 and 7-O-Methylwogonin; (L) AKT1 and 5-Hydroxy-7,2',3'-Trimethoxyflavone; (M) PIK3R1 and 5-Hydroxy-7,8,2',5'-Tetramethoxyflavone; and (N) HSD11B1 and 5-Hydroxy-7,2',3'-Trimethoxyflavone

MAPK3 were also found to activate ERK2 and ERK1, respectively, contributing to the ERK1/2 pathway. Upregulated ERK1/2 pathway was reported to be involved in the activation of pro-inflammatory mediators in skin photoaging, including

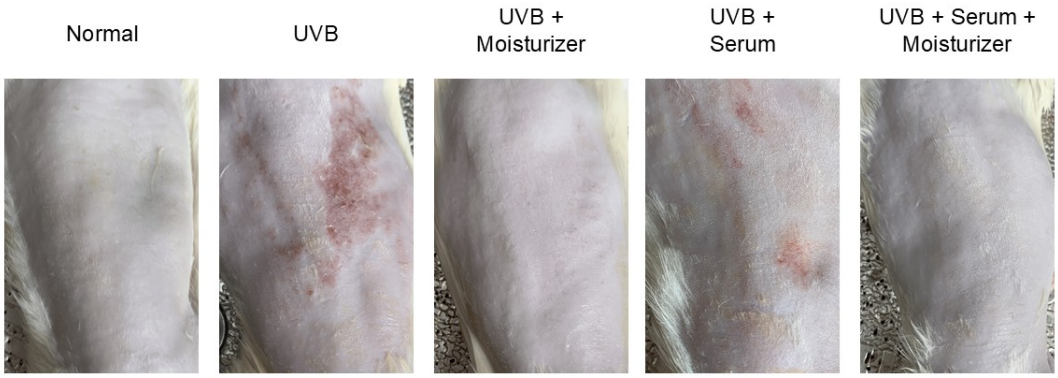


**Figure 8.** Dorsal Images of Rat Skin

the COX-2 (Muralitharan et al., 2025). JNKs, particularly activated by MAPK8 and MAPK10, were also demonstrated to regulate the expression of MMP-1 and Cx43, triggering the degradation of collagen and extracellular matrix, ultimately leading to accelerated organismal skin aging (Li et al., 2024).

The nuclear activity of NF-$\kappa$B induce several mediators associated with inflammation-related mechanism of the skin, including the interleukins (ILs) and cyclooxygenase (COX)-2 (Wang et al., 2020). The phosphoinositide 3-kinases (PI3Ks) were studied for its role in maintaining skin homeostasis by inhibiting ROS production. UVB-induced skin photoaging triggers the modification of PI3K signaling pathway, therefore enabling the overproduction of ROS within human dermal fibroblasts (Noh et al., 2016). However, PI3K were also reported to upregulate MMP-1 expression, leading to the degradation of collagen. Therefore, targeting PI3K might provide favorable anti-photoaging activities (Kim et al., 2020). The downstream activation of PI3K also initiate several cascades of signaling pathways, including the activation of protein kinase B (Akt), which was implicated in several immunological- and aging-related pathological conditions (Fruman et al., 2017).

11$\beta$-hydroxysteroid dehydrogenases (HSD11B) are implicated in the aging and inflammation of skin tissue. While HSD11B2 conformation were reported to inactivate cortisol, HSD11B1 were widely found within both the skin epidermis and dermis. HSD11B1 was reported to be responsible in regulating glucocorticoid hormone within the skin, particularly in activating cortisol. Overexposure of UVB radiation may trigger the upregulation of HSD11B1 activity, indicating its role in skin photoaging and potential of becoming a target for photoaging therapies (Tiganescu et al., 2011).

### 3.5 Effect of Moisturizer and Serum to Epidermal Thickness, DEJ Flattening, and Collagen Density in UVB-Induced Photoaging

Photoaging of skin is characterized by increased epidermal thickness and degradation of collagen structure. A histological assessment of the dorsal skin in hairless rats was carried out to evaluate the photoaging effects of the formulations on epidermal thickness and collagen density. H&E staining revealed that UVB exposure significantly increased epidermal thickness ($p<0.05$). Rats treated with moisturizer and serum displayed a decreased skin thickness ($p<0.05$) (Figures 8 and 9B). Masson's trichrome stain was employed to visualize collagen fibers, which stain blue (Figure 9A). Collagen density was significantly reduced in the UVB control group compared to the normal group ($p<0.05$), whereas collagen preservation was higher in tissues from rats treated with the formulations than in the UVB- group ($p<0.05$) (Figure 9D). These findings indicate that serum and moisturizer may inhibit collagen degradation and alleviate the impact of UVB irradiation on epidermal thickening.

This study provides evidence that topical applications of serum and moisturizer formulated with *Andrographis paniculata* extract, clove oil, and patchouli oil can mitigate structural skin damage associated with UVB-induced photoaging. H&E staining revealed a marked elevation in epidermal thickness in the UVB-exposed animals when compared to the normal control group, indicating photoaging-induced hyperplasia. Quantitative analysis showed that treatment with serum, moisturizer, or their combination significantly lowered epidermal thicknening in comparison with the UVB-only group. Among the treated groups, the combination of serum and moisturizer demonstrated the greatest reduction in epidermal thickness, approaching values similar to the normal group. The histological images confirmed these findings, showing compact and less hyperproliferative epidermal layers in treated samples compared to the UVB-exposed group, which exhibited pronounced thickening of the stratum spinosum and disorganization of the basal layer. The observed reduction in epidermal thickness following topical application of serum and moisturizer formulations is consistent with prior studies reporting the photoprotective effects of botanical extracts. *Andrographis paniculata* suppresses epidermal hyperproliferation through the inhibition of inflammatory cytokines and oxidative stress pathways (Fardiyah et al.,

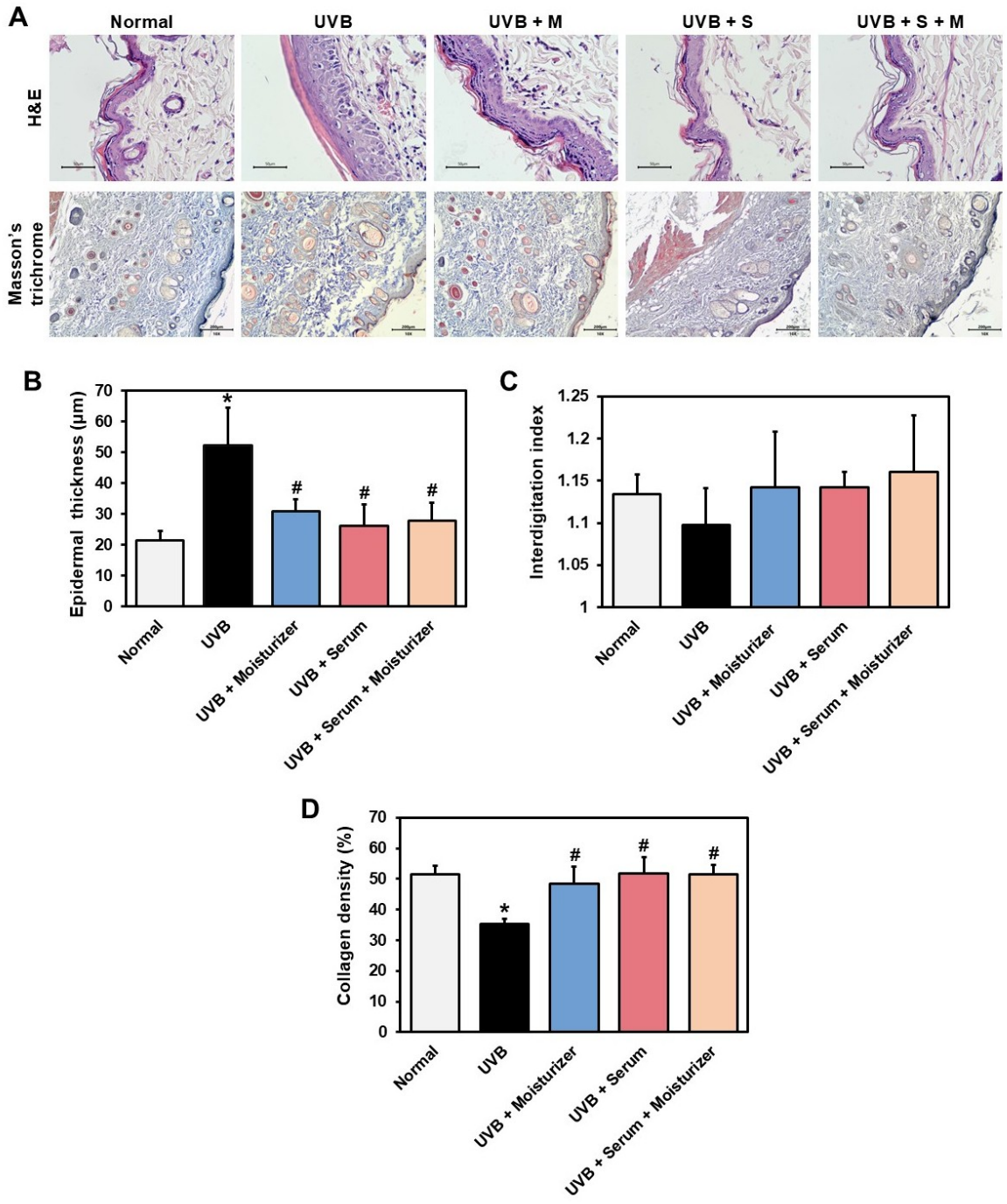


**Figure 9.** Histological Analysis. (A) H&E and Masson's Trichrome Stained Section; (B) Epidermal Thickness; (C) Interdigitation Index; (D) Collagen Density. *P <0.05 Vs Normal Group. #P <0.05 Vs UVB Group

2020). Similarly, eugenol, the active compound in *Syzygium aromaticum*, has been shown to regulate keratinocyte proliferation and enhance epidermal barrier function (Hwang et al., 2018). Patchouli oil from *Pogostemon cablin* has also demonstrated anti-inflammatory activity and the ability to normalize epidermal turnover under UV-induced stress (Feng et al., 2014). The current results extend these findings by demonstrating that the combination of these herbals yields an enhanced effect, suggesting potential synergism in reducing UVB-induced epidermal alterations. The ability of the tested formulations to attenuate UVB-induced epidermal thickening suggests that these products may contribute to the preservation of epidermal

homeostasis under photo-oxidative stress. Since epidermal hyperplasia is an early marker of photoaging and a precursor to more severe histological damage, such as collagen breakdown and dermo-epidermal junction (DEJ) flattening, the observed protective effect is of significant dermatological relevance.

Histological examination of the DEJ revealed substantial flattening and loss of interdigitation in the UVB-only group, indicating disruption of the structural interface between the epidermis and dermis. Although quantitative analysis of the interdigitation index did not show statistically significant differences among groups ($p>0.05$) (Figure 9C), qualitative observations suggested that treatment with serum, moisturizer, or their combination preserved the undulating pattern of the DEJ more effectively than UVB exposure alone. The combination group exhibited the most consistent retention of rete ridges and dermal papillae, suggesting a protective trend. These findings are noteworthy as the integrity of the DEJ is crucial for mechanical stability, nutrient exchange, and epidermal anchoring. The apparent preservation of this structure by the tested formulations may be attributed to the synergistic antioxidant and anti-inflammatory actions of their botanical components, which attenuate the UVB-induced degradation of dermal-epidermal adhesion molecules (Costa et al., 2022; Jain et al., 2023).

Masson's trichrome staining demonstrated a marked reduction in collagen density in the UVB-irradiated group, consistent with the known catabolic effects of ultraviolet radiation on dermal extracellular matrix components. Treatment with serum, moisturizer, and their combination significantly improved collagen preservation, as indicated by denser and more uniformly distributed blue-stained collagen fibers in the dermis. The combination group yielded the highest collagen density among the treated groups, approaching the level observed in the normal control group. These findings align with previous reports that *Andrographis paniculata* can suppress MMP-mediated collagen degradation via inhibition of pro-inflammatory and oxidative signaling cascades (Fardiyah et al., 2020), while *Syzygium aromaticum* and *Pogostemon cablin* enhance fibroblast activity and collagen synthesis (Feng et al., 2014). The ability of the topical formulations to restore collagen content highlights their therapeutic potential in delaying the structural consequences of photoaging. The consistency of this result with the epidermal thickness reduction further reinforces the efficacy of the products in mitigating both superficial and dermal manifestations of chronic UVB exposure.

## 4. CONCLUSIONS

This study showed that topical application of serum and moisturizer containing *Andrographis paniculata* extract, clove oil, and patchouli oil effectively mitigated UVB-induced photoaging in Wistar rats. The formulations significantly reduced epidermal thickness and preserved collagen density, while also showing a potential to maintain the structural integrity of the dermo-epidermal junction. The results provide promising preclinical evidence for the advancing natural and plant-based skincare products with anti-aging properties. Future investigations are recommended to clarify the molecular mechanisms underlying these effects and to validate their efficacy in human clinical settings.

## 5. ACKNOWLEDGMENT

This study was funded by the Ministry of Research, Technology, and Higher Education of the Republic of Indonesia with Grant No. 0599/E/KS.03.00/2023 through the Matching Fund Program 2023. The authors sincerely thank PT. Skinpharma Teknologi Indonesia for providing the serum and moisturizer formulations used in this research. We also acknowledge the Laboratory of Pharmacology and the Laboratory of Pathology Anatomy, Faculty of Medicine, Universitas Brawijaya, for their valuable support in conducting the *in vivo* experiment and histological analysis.

## REFERENCES

Addas, A., M. Ragab, A. Maghrabi, S. M. Abo-Dahab, and E. F. El-Nobi (2021). UV Index for Public Health Awareness Based on OMI/NASA Satellite Data at King Abdulaziz University, Saudi Arabia. *Advances in Mathematical Physics*, **1**; 2835393

Adianingsih, O. R., F. F. Fajrin, and C. K. Johan (2024). Exploring the Mechanism of *Glycyrrhiza glabra* and *Curcuma domestica* Against Skin Photoaging Based on Network Pharmacology. *Indonesian Journal of Biotechnology*, **29**(2); 98–110

Anawalt, B. D. and A. M. Matsumoto (2022). Aging and Androgens: Physiology and Clinical Implications. *Reviews in Endocrine and Metabolic Disorders*, **23**(6); 1123–1137

Anjum, M. M., D. N. Kumar, S. Bhattacharya, K. K. Patel, M. R. Vijayakumar, A. K. Agrawal, and S. Singh (2023). Topical Delivery of Cyclodextrin Crosslinked Nanosponge of Anacardic Acid for Treatment of UV-B Induced Skin Photoaging: Formulation, Characterization and Biochemical Estimation. *Journal of Drug Delivery Science and Technology*, **87**; 104840

Benet, L. Z., C. M. Hosey, O. Ursu, and T. I. Oprea (2016). BDDCS, the Rule of 5 and Drugability. *Advanced Drug Delivery Reviews*, **101**; 89–98

Bosch, R., N. Philips, J. A. Suárez-Pérez, A. Juarranz, A. Devmurari, J. Chalensouk-Khaosaat, and S. González (2015). Mechanisms of Photoaging and Cutaneous Photocarcinogenesis, and Photoprotective Strategies with Phytochemicals. *Antioxidants*, **4**(2); 248–268

Cavinato, M., B. Waltenberger, G. Baraldo, C. V. C. Grade, H. Stuppner, and P. Jansen-Dürr (2017). Plant Extracts and Natural Compounds Used Against UVB-Induced Photoaging. *Biogerontology*, **18**(4); 499–516

Chang, K. C. N., Y. Wang, I. G. Oh, S. Jenkins, L. P. Freedman, C. C. Thompson, J. H. Chung, and S. Nagpal (2010). Estrogen Receptor $\beta$ Is a Novel Therapeutic Target for Photoaging. *Molecular Pharmacology*, **77**(5); 744–750

Charles-De-Sá, L., N. Gontijo-De-Amorim, A. Sbarbati, D. Benati, P. Bernardi, R. Borojevic, R. B. V. Carias, and

 

G. Rigotti (2020). Photoaging Skin Therapy with PRP and ADSC: A Comparative Study. *Stem Cells International*

Chauhan, E. S., K. Sharma, and R. Bist (2019). Andrographis Paniculata: A Review of Its Phytochemistry and Pharmacological Activities. *Research Journal of Pharmacy and Technology*, **12**(2); 891–900

Chen, W., Q. Deng, B. Deng, Y. Li, G. Fan, F. Yang, W. Han, J. Xu, and X. Chen (2024). Comprehensive Analysis of *Hibisci mutabilis folium* Extract's Mechanisms in Alleviating UV-Induced Skin Photoaging Through Enhanced Network Pharmacology and Experimental Validation. *Frontiers in Pharmacology*, **15**; 1431391

Chmielewski, R. and A. Lesiak (2024). Mitigating Glycation and Oxidative Stress in Aesthetic Medicine: Hyaluronic Acid and Trehalose Synergy for Anti-AGEs Action in Skin Aging Treatment. *Clinical, Cosmetic and Investigational Dermatology*, **17**; 2701–2712

Costa, E. F., W. V. Magalhães, and L. C. Di Stasi (2022). Recent Advances in Herbal-Derived Products with Skin Anti-Aging Properties and Cosmetic Applications. *Molecules*, **27**(21); 7518

Daina, A., O. Michielin, and V. Zoete (2017). SwissADME: A Free Web Tool to Evaluate Pharmacokinetics, Drug-Likeness and Medicinal Chemistry Friendliness of Small Molecules. *Scientific Reports*, **7**(1); 42717

Damayanti, C. Prakoeswa, D. Purwanto, A. Endaryanto, M. Listiawan, Y. Wirohadidjoyo, Soetjipto, Siswandono, and B. Utomo (2023). Wistar Rat as Photoaging Mouse Model. *Journal of Pakistan Association of Dermatologists*, **33**(1); 24–29

Deng, Q., W. Chen, B. Deng, W. Chen, L. Chen, G. Fan, J. Wu, Y. Gao, and X. Chen (2024). Based on Network Pharmacology, Molecular Docking and Experimental Verification to Reveal the Mechanism of *Andrographis paniculata* Against Solar Dermatitis. *Phytomedicine*, **135**; 156025

Dibal, N. I., S. H. Garba, and T. W. Jacks (2022). Histological Stains and Their Application in Teaching and Research. *Asian Journal of Health Sciences*, **8**(2); 43–43

Fardiyah, Q., T. Ersam, Suyanta, A. Slamet, Suprapto, and F. Kurniawan (2020). New Potential and Characterization of *Andrographis paniculata* L. Ness Plant Extracts as Photoprotective Agent. *Arabian Journal of Chemistry*, **13**(12); 8888–8897

Feng, C., X. Chen, X. Yin, Y. Jiang, and C. Zhao (2024). Matrix Metalloproteinases on Skin Photoaging. *Journal of Cosmetic Dermatology*, **23**(12); 3847–3862

Feng, X. X., X. T. Yu, W. J. Li, S. Z. Kong, Y. H. Liu, X. Zhang, Y. F. Xian, X. J. Zhang, Z. R. Su, and Z. X. Lin (2014). Effects of Topical Application of Patchouli Alcohol on the UV-Induced Skin Photoaging in Mice. *European Journal of Pharmaceutical Sciences*, **63**; 113–123

Ferreira, M. S., M. C. Magalhães, R. Oliveira, J. M. Sousa-Lobo, and I. F. Almeida (2021). Trends in the Use of Botanicals in Anti-Aging Cosmetics. *Molecules*, **26**(12)

Freitas-Rodríguez, S., A. R. Folgueras, and C. López-Otín (2017). The Role of Matrix Metalloproteinases in Aging: Tissue Remodeling and Beyond. *Biochimica et Biophysica Acta - Molecular Cell Research*, **1864**(11); 2015–2025

Fruman, D. A., H. Chiu, B. D. Hopkins, S. Bagrodia, L. C. Cantley, and R. T. Abraham (2017). The PI3K Pathway in Human Disease. *Cell*, **170**(4); 605–635

Fuller, B. (2019). Role of PGE-2 and Other Inflammatory Mediators in Skin Aging and Their Inhibition by Topical Natural Anti-Inflammatories. *Cosmetics*, **6**(1); 6

Galovičová, L., P. Borotová, V. Valková, H. Ďúranová, J. Štefániková, N. L. Vukovic, M. Vukic, and M. Kačániová (2022). Biological Activity of Pogostemon Cablin Essential Oil and Its Potential Use for Food Preservation. *Agronomy*, **12**(2); 387

Gao, X., F. Luo, and H. Zhao (2021). Cloves Regulate $Na^+$-$K^+$-ATPase to Exert Antioxidant Effect and Inhibit UVB Light-Induced Skin Damage in Mice. *Oxidative Medicine and Cellular Longevity*, **1**; 5197919

Gong, M., P. Zhang, C. Li, X. Ma, and D. Yang (2018). Protective Mechanism of Adipose-Derived Stem Cells in Remodelling of the Skin Stem Cell Niche During Photoaging. *Cellular Physiology and Biochemistry*, **51**(5); 2456–2471

Han, M., H. Li, D. Ke, L. M. Tian, Y. Hong, C. Zhang, D. Z. Tian, L. Chen, L. R. Zhan, and S. Q. Zong (2022a). Mechanism of Ba Zhen Tang Delaying Skin Photoaging Based on Network Pharmacology and Molecular Docking. *Clinical, Cosmetic and Investigational Dermatology*, **15**; 763–781

Han, S. H., E. Ballinger, S. Y. Choung, and J. Y. Kwon (2022b). Anti-Photoaging Effect of Hydrolysates from Pacific Whiting Skin via MAPK/AP-1, NF-kB, TGF-$\beta$/Smad, and Nrf-2/HO-1 Signaling Pathway in UVB-Induced Human Dermal Fibroblasts. *Marine Drugs*, **20**(5); 308

Hani, R., L. Khayat, A. A. Rahman, and N. Alaaeddine (2023). Effect of Stem Cell Secretome in Skin Rejuvenation: A Narrative Review. *Molecular Biology Reports*, **50**(9); 7745–7758

Harnelly, E., A. H. Halym, N. Isnaini, K. Khairan, Z. Zulkarnain, A. Syahraini, W. Sari, H. Maghfira, S. Muhammad, R. Idrus, and M. El-Shazly (2025). Protective Effects of Crude and Light Fraction Patchouli Oil Against UVB-Induced Dermal Aging in Mice: In Silico and In Vivo Study. *Trends in Sciences*, **22**(12); 10723

Hema, K., S. Ahamad, H. K. Joon, R. Pandey, and D. Gupta (2021). Atomic Resolution Homology Models and Molecular Dynamics Simulations of Plasmodium Falciparum Tubulins. *ACS Omega*, **6**(27); 17510–17522

Huang, J., Y. Gong, K. Liu, J. Chen, and X. Zhou (2023). Anti-Photoaging Properties of Asiaticoside in Ultraviolet A-Irradiated Human Dermal Fibroblasts by Activating the PI3K-AKT Pathway and Inhibiting the NF-kB Pathway. *Exploratory Research and Hypothesis in Medicine*, **000**(000); 319–337

Hwang, E., P. Lin, H. T. T. Ngo, and T. H. Yi (2018). Clove Attenuates UVB-Induced Photodamage and Repairs Skin Barrier Function in Hairless Mice. *Food and Function*, **9**(9); 4936–4947

 

Intharuksa, A., W. Arunotayanun, W. Yooin, and P. Sirisa-ard (2022). A Comprehensive Review of *Andrographis paniculata* (Burm. f.) Nees and Its Constituents as Potential Lead Compounds for COVID-19 Drug Discovery. *Molecules*, **27**(14); 4479

Jain, A. N. and A. Nicholls (2008). Recommendations for Evaluation of Computational Methods. *Journal of Computer-Aided Molecular Design*, **22**(3–4); 133–139

Jain, R., R. Yadav, S. P. Tiwari, and J. Swarnkar (2023). An Overview of Medicinal Plants Used for Anti-Aging Face Pack Formulation. *Journal of Pharmaceutical Negative Results*, **14**(2); 2023

Kim, D. E., Y. S. Hwang, B. Y. Chang, D. S. Kim, H. K. Cho, and S. Y. Kim (2019). Effects of the *Syzygium aromaticum* L. Extract on Antioxidation and Inhibition of Matrix Metalloproteinase in Human Dermal Fibroblast. *Asian Pacific Journal of Tropical Biomedicine*, **9**(2); 53–59

Kim, D. H., J. H. Auh, J. Oh, S. Hong, S. Choi, E. J. Shin, S. O. Woo, T. G. Lim, and S. Byun (2020). Propolis Suppresses UV-Induced Photoaging in Human Skin Through Directly Targeting Phosphoinositide 3-Kinase. *Nutrients*, **12**(12); 1–12

Lephart, E. D. and F. Naftolin (2022). Factors Influencing Skin Aging and the Important Role of Estrogens and Selective Estrogen Receptor Modulators (SERMs). *Clinical, Cosmetic and Investigational Dermatology*, **15**; 1695–1709

Li, W., A. Shih, Y. Freudenberg-Hua, W. Fury, and Y. Yang (2021). Beyond Standard Pipeline and P < 0.05 in Pathway Enrichment Analyses. *Computational Biology and Chemistry*, **92**; 107455

Li, Y., L. You, E. Nepovimova, V. Adam, Z. Heger, K. Jomova, M. Valko, Q. Wu, and K. Kuca (2024). C-Jun N-Terminal Kinase Signaling in Aging. *Frontiers in Aging Neuroscience*, **16**; 107455

Liu, H., J. Dong, R. Du, Y. Gao, and P. Zhao (2024). Collagen Study Advances for Photoaging Skin. *Photodermatology, Photoimmunology and Photomedicine*, **40**(1); e12931

Manosalva, C., P. Alarcón, L. Grassau, C. Cortés, J. L. Hancke, and R. A. Burgos (2025). Andrographolide Mitigates Inflammation and Reverses UVB-Induced Metabolic Reprogramming in HaCaT Cells. *International Journal of Molecular Sciences*, **26**(13); 6508

Mohiuddin, A. (2019). Skin Aging & Modern Age Anti-Aging Strategies. *International Journal of Clinical Dermatology & Research*; 209–240

Muralitharan, R. V., S. F. Masre, D. F. Basri, and A. R. Ghazali (2025). Pterostilbene and Resveratrol: Exploring Their Protective Mechanisms Against Skin Photoaging – A Scoping Review. *Biochemistry and Biophysics Reports*, **42**

Mutiah, R., M. S. D. Briliana, A. R. A. Ahmad, B. Fauziyah, N. A. Janaloka, and A. Suryadinata (2024). Network Pharmacology and Component Analysis Integrated Study to Uncovers the Molecular Mechanisms of *Lansium parasiticum* Bark Extract in Colon Cancer Treatment. *Science and Technology Indonesia*, **9**(2); 314–324

Noh, E. M., J. Park, H. R. Song, J. M. Kim, M. Lee, H. K. Song, O. Y. Hong, P. H. Whang, M. K. Han, K. B. Kwon, J. S. Kim, and Y. R. Lee (2016). Skin Aging-Dependent Activation of the PI3K Signaling Pathway via Downregulation of PTEN Increases Intracellular ROS in Human Dermal Fibroblasts. *Oxidative Medicine and Cellular Longevity*

Pandey, V. K., S. Srivastava, Ashish, K. K. Dash, R. Singh, A. H. Dar, T. Singh, A. Farooqui, A. M. Shaikh, and B. Kovacs (2024). Bioactive Properties of Clove (*Syzygium aromaticum*) Essential Oil Nanoemulsion: A Comprehensive Review. *Heliyon*, **10**(1); e22437

Pangestuti, R., K. H. Shin, and S. K. Kim (2021). Anti-Photoaging and Potential Skin Health Benefits of Seaweeds. *Marine Drugs*, **19**(3); 172

Sharma, R. R., A. Deep, and S. T. Abdullah (2022). Herbal Products as Skincare Therapeutic Agents Against Ultraviolet Radiation-Induced Skin Disorders. *Journal of Ayurveda and Integrative Medicine*, **13**(1); 100500

Tiganescu, A., E. A. Walker, R. S. Hardy, A. E. Mayes, and P. M. Stewart (2011). Localization, Age- and Site-Dependent Expression, and Regulation of 11$\beta$-Hydroxysteroid Dehydrogenase Type 1 in Skin. *Journal of Investigative Dermatology*, **131**(1); 30–36

Urdiales-Gálvez, F., S. Martín-Sánchez, M. Maíz-Jiménez, A. Castellano-Miralla, and L. Lionetti-Leone (2019). Concomitant Use of Hyaluronic Acid and Laser in Facial Rejuvenation. *Aesthetic Plastic Surgery*, **43**(4); 1061–1070

Wang, M. L., Q. Y. Zhong, B. Q. Lin, Y. H. Liu, Y. F. Huang, Y. Chen, J. Yuan, Z. R. Su, and J. Y. X. Zhan (2020). Andrographolide Sodium Bisulfate Attenuates UV-Induced Photo Damage by Activating the Keap1/Nrf2 Pathway and Downregulating the NF kB Pathway in HaCaT Keratinocytes. *International Journal of Molecular Medicine*, **45**(2); 343–352

Wang, X., B. Teferedegne, K. Shatzkes, W. Tu, and H. Murata (2016). Endogenous RNase Inhibitor Contributes to Stability of RNA in Crude Cell Lysates: Applicability to RT-qPCR. *Analytical Biochemistry*, **513**; 21–27

Wang, Y., Q. Zhang, H. Liao, X. Lu, J. Cong, Z. Liu, Q. Liu, C. Deng, Y. Cheng, P. Shu, and Q. Xiang (2025). Anti Photoaging Mechanism of a Novel Recombinant Human Fibronectin Peptide (rhFNP) Derived from the Extracellular Matrix. *Heliyon*, **11**(4); e42730

Whitty, A., M. Zhong, L. Viarengo, D. Beglov, D. R. Hall, and S. Vajda (2016). Quantifying the Chameleonic Properties of Macrocycles and Other High-Molecular-Weight Drugs. *Drug Discovery Today*, **21**(5); 712–717

Wong, F., A. Krishnan, E. J. Zheng, H. Stärk, A. L. Manson, A. M. Earl, T. Jaakkola, and J. J. Collins (2022). Benchmarking AlphaFold-Enabled Molecular Docking Predictions for Antibiotic Discovery. *Molecular Systems Biology*, **18**(9); e11081

Xu, D. and M. Zhao (2022). Photoaging Induced by Long-Term Exposure to UV Irradiation and Amelioration by Skipjack Tuna Skin Hydrolysates: Targeting Inhibition of MAPK and NF-kB Signaling Hyperactivation. *Journal of Functional*

 

*Foods*, **98**; 105281

Xu, J., G. Wu, X. Yu, Z. Dong, J. Yan, L. Wu, L. Bao, and Q. Liu (2023). Exploring the Mechanism of MP Gel Against Skin Photoaging Based on Network Pharmacology, Molecular Docking, and Experimental Validation. *Journal of Cosmetic Dermatology*, **22**(3); 1108–1123

Zhan, J. Y. X., X. F. Wang, Y. H. Liu, Z. B. Zhang, L. Wang, J. N. Chen, S. Huang, H. F. Zeng, and X. P. Lai (2016). Andrographolide Sodium Bisulfate Prevents UV-Induced Skin Photoaging Through Inhibiting Oxidative Stress and Inflammation. *Mediators of Inflammation*, **1**; 3271451

 